Chinese Science Bulletin 2006 Vol. 51 No. 13 1639—1643

DOI: 10.1007/s11434-006-2013-4

Deformation behavior during nanoindentation in Ce-based bulk metallic glasses

ZHANG Lingchen[1], XING Dongmei[2,3], ZHANG Taihua[2], WEI Bingchen[1], LI Weihuo[1] & WANG Yuren[1]

1. National Microgravity Laboratory, Institute of Mechanics, Chinese Academy of Sciences, Beijing 100080, China;
2. State Key Laboratory of Nonlinear Mechanics (LNM), Institute of Mechanics, Chinese Academy of Sciences, Beijing 100080, China;
3. College of Physics and Electronic Information Science, Tianjin Normal University, Tianjin 300072, China

Correspondence should be addressed to Wei Bingchen (email: weibc@imech.ac.cn)

Received December 27, 2005; accepted January 23, 2006

Abstract The deformation behavior and the effect of the loading rate on the plastic deformation in Ce-based bulk metallic glasses (BMGs) were investigated through nanoindentation tests. The results showed that the loading rate dependence of plastic deformation during nanoindentation measurements in the Ce-based BMGs is quite unique in contrast to that of other BMG alloys. The load-displacement (*P-h*) curves of $Ce_{60}Al_{15}Cu_{10}Ni_{15}$ BMG exhibit a homogeneous plastic deformation at low loading rates, and a prominent serrated flow at high strain rates, whereas, the *P-h* curves of $Ce_{65}Al_{10}Cu_{10}Ni_{10}Nb_5$ exhibit homogenous plastic deformation at all studied loading rates. The room temperature creep behavior could clearly be observed in these two alloys. The mechanism of the unique plastic deformation feature in the Ce-based BMGs was studied.

Keywords: bulk metallic glass, nanoindentation, serrated flow, creep.

Recently, bulk metallic glasses (BMGs) have attracted a great deal of attention due to their extremely high strength, improved wear resistance and excellent corrosion resistance[1−7]. However, it is known that their structural applications are currently limited by the lack of significant plastic deformation at room temperature. Therefore, the deformation mechanism and the improvement of plasticity of BMGs are two active topics in this area[4−7]. More recently, more and more nanoindentation experiments have been performed to evaluate the mechanical response of metallic glasses, considering their superiority of allowing considerably larger plastic deformation to be accumulated in the quasi-brittle materials in a localized area around the indented regions[8−13]. Golovin and Schuh *et al.* observed serrated flow phenomenon in load-displacement (P-h) curves of Pd-, Zr-, La- and Mg-based BMGs during nanoindentation[8−13]. It is supposed that the serrated flow is correlated with the formation and propagation of shear bands, and the features of serrated flow depend strongly on the chemical composition, applied strain rate and microstructure of BMGs[8−13]. At the same strain rate, the Pd-based alloys exhibit sharper serrations than the Zr-based alloys. Furthermore, the serrated flow is pronounced at lower strain rates and is suppressed at high strain rates for the same BMGs system. Schuh *et al.* found that at low strain rates individual shear bands would discretely accommodate the plastic deformation, while at high strain rates multiple shear bands would be activated instantaneously, leading to a homogenous deformation[8,9,12,13]. This result is nominally counterintuitive, as metallic glasses are well known to exhibit inhomogeneous flow at high strain rates[14,15]. Greer *et al.* suggested that the homogenous plastic deformation behavior at high strain rates is due to the lack of resolution of the instruments at high loading rates[16]. Therefore, more detailed work is needed to clarify this controversy. This is also important for the understanding of the plastic deformation mechanism in BMGs. In this work, the plastic deformation behavior of Ce-based BMGs with quite low glass transition temperature (T_g)[17] was studied via nanoindentation. The effect of strain rates on deformation behavior was also studied in this alloy system. An anomalous strain rate dependency of serrated flow in the Ce-based BMGs during nanoindentation is reported and discussed here.

1 Experimental

Ingots of $Ce_{60}Al_{15}Cu_{10}Ni_{15}$ and $Ce_{65}Al_{10}Cu_{10}Ni_{10}Nb_5$ alloys were prepared by arc-melting the pure elements together under a purified argon atmosphere, and cast into a copper mold with a dimension of 5×2×55 mm^3. The structure of the samples was characterized by X-ray diffraction (XRD) using Cu $K\alpha$ radiation. Thermal analysis was performed with a Perkin-Elmer DSC 7 differential scanning calorimeter at a heating rate of 20 K/min under argon atmospheres. Nanoindentation tests were conducted using an MTS Nano Indenter XP^{TM} with a Berkovich diamond tip, and through load-

ing control mode. Nanoindentation experiments consisted of five subsequent steps: loading to a peak depth at the setting loading rate, holding the load for 10 s at the peak depth, then unloading 90% of peak load at the unloading rate same to the loading one, followed by holding load for 10 s, and finally unloading completely. Five loading rates were used in the experiments (0.03 mN/s, 0.075 mN/s, 0.2 mN/s, 0.5 mN/s and 1 mN/s). All the tests were carried out at room temperature (296 K). The surfaces of specimens after nanoindentation tests were observed by Olympus BX61 optic microscope.

2 Results and discussion

The DSC results obtained at a heating rate of 20 K/min of the as-cast $Ce_{60}Al_{15}Cu_{10}Ni_{15}$ and $Ce_{65}Al_{10}Cu_{10}Ni_{10}Nb_5$ samples are presented in Fig. 1. The two alloys both show an endothermic reaction caused by glass transition, followed by an exothermic reaction caused by crystallization. The onset temperature of glass transition (T_g), the crystallization temperature (T_x) and the width of supercooled liquid region ($\Delta T=T_x-T_g$) of the $Ce_{60}Al_{15}Cu_{10}Ni_{15}$ alloy are 410.3 K, 478.3 K and 68 K respectively, and 355.2 K, 389.1 K and 33.9 K respectively for the $Ce_{65}Al_{10}Cu_{10}Ni_{10}Nb_5$ alloy. The inset of Fig. 1 exhibits the XRD results of the two alloys, characteristic of amorphous phase without obvious crystalline reflection peaks.

The load-displacement (*P-h*) curves of $Ce_{60}Al_{15}Cu_{10}Ni_{15}$ and $Ce_{65}Al_{10}Cu_{10}Ni_{10}Nb_5$ BMGs during nanoindentation at various loading rates are presented in Fig. 2. The origin of each curve is displaced for clear observation. Fig. 2(a) shows that the *P-h* curves of the $Ce_{60}Al_{15}Cu_{10}Ni_{15}$ alloy depend strongly on the applied loading rates. The loading part of the *P-h* curve is smooth at the low loading rates, but exhibits prominent serrated flow with increasing loading rates. The critical loading rate for the appearance of the serrated flow is 0.2 mN/s. Furthermore, Fig. 2(a) also reveals creep during the load holding segment for 10 s at the maximum load. This is more prominent at higher loading rates (about 30 nm at 1.0 mN/s). Fig. 2(a) also shows that the maximum load at an indentation depth of 1000 nm increases with increasing loading rate. This means that the hardness of the alloy strongly depends on the loading rate, and increases gradually from 1.75 GPa at 0.03 mN/s to 2.45 GPa at 1.0 mN/s. *P-h* curves for nanoindentations on the $Ce_{65}Al_{10}Cu_{10}Ni_{10}Nb_5$ BMG at various loading rates are presented in Fig. 2(b). It is shown that the *P-h* curves at all the studied loading rates are smooth without distinct serrations. Further-

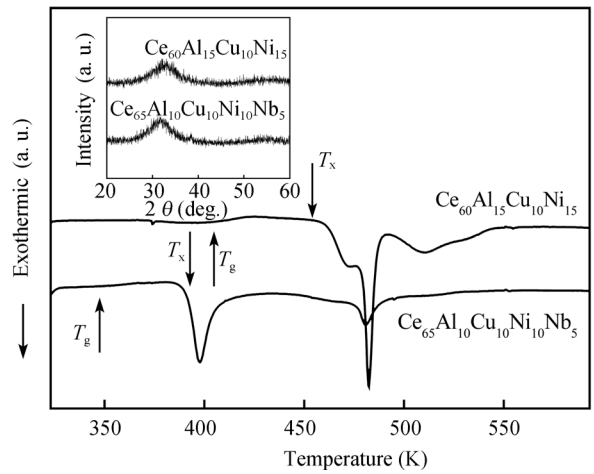

Fig. 1. DSC curves for the $Ce_{60}Al_{15}Cu_{10}Ni_{15}$ and $Ce_{65}Al_{10}Cu_{10}Ni_{10}Nb_5$ BMGs at the heating rate of 20 K/min. The inset is XRD patterns for the two BMGs.

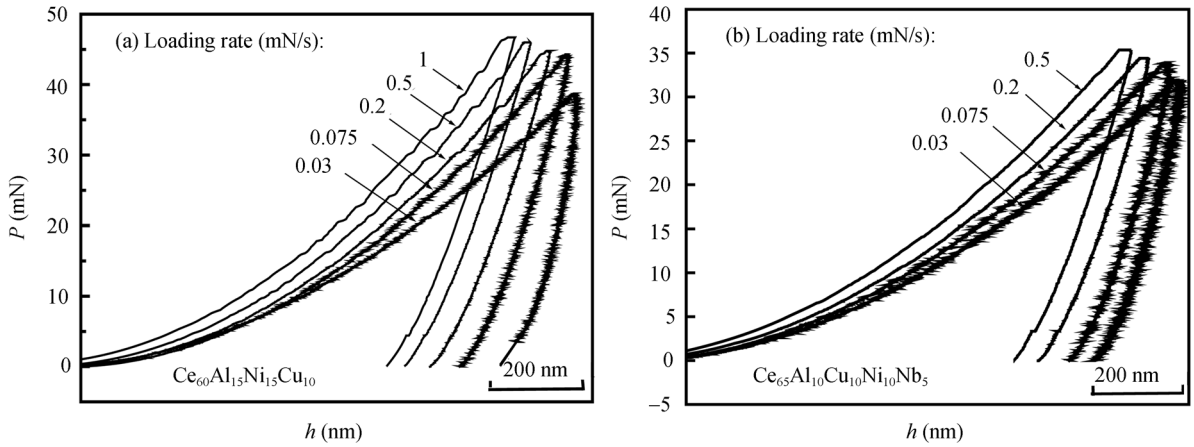

Fig. 2. Typical load-displacement (*P-h*) curves during nanoindentation at various loading rates for $Ce_{60}Al_{15}Cu_{10}Ni_{15}$ (a) and $Ce_{65}Al_{10}Cu_{10}Ni_{10}Nb_5$ (b).

more, the creep displacements are also observed in $Ce_{65}Al_{10}Cu_{10}Ni_{10}Nb_5$ BMG during the holding load segment with the displacement of the creep increasing with the increase of the loading rate. In addition, the hardness of the $Ce_{65}Al_{10}Cu_{10}Ni_{10}Nb_5$ alloy also increases with increasing loading rate.

The serrated flow during nanoindentation has already been investigated in the *P-h* curves in Pd-, Zr-, La- and Mg-based BMGs[8−13]. In these alloy systems, the *P-h* curves exhibited numerous serrations or pronounced discrete steps at low strain rates, and these serrations became less prominent or totally disappeared as the strain rate is increased. Schuh *et al.* indicated that the serrations were correlated with the operation and propagation of shear bands. At low loading rates, single shear bands operate in isolation and propagate sufficiently, whereas at high rates there were many shear bands operating within the specimen at the same instant, corresponding to the unconspicuous serrations. In contrast, the present $Ce_{60}Al_{15}Cu_{10}Ni_{15}$ alloy exhibits an anomalous rate dependency of the serrated flow during nanoindentation, i.e. the alloy exhibits a smooth loading curve at low rates and pronounced serrations at high rates. This suggests that the mechanism for the serrated flow is different in different BMG systems.

The anomalous serrated flow phenomenon in $Ce_{60}Al_{15}Cu_{10}Ni_{15}$ alloy may be associated with the yield drop, as was observed by Kawamura, Chen, Nieh *et al.* in compressive experiment near T_g in Zr-, Pd-based BMGs [18−21]. That is, the flow stress (σ) increases initially to a maximum (σ_{yield}), then decreases and finally attains a steady-state flow value, σ_{flow}. The magnitude of the yield drop ($\Delta\sigma=\sigma_{yield}-\sigma_{flow}$) depends strongly on temperature and strain rate. During constant strain-rate tests, $\Delta\sigma$ shows a higher value at relatively low temperature or high strain rate[19]. The appearance of the serrated flow in $Ce_{60}Al_{15}Cu_{10}Ni_{15}$ alloy at high loading rates may be related to the yield drop phenomenon. The yield drop is a result of rapid increase in free volume during high stain rate deformation. Under a continuous loading, a great deal of free volume is produced, thus relaxing the stress concentration. An increase in free volume caused by the strain competes with a decrease in free volume caused by diffusion until an equilibrium state is reached (σ_{flow}). The diffusion is a time-dependent process; thus the decrease in free volume is suppressed at the high loading rates, and the yield drop phenomenon is more prominent. On the other hand, the yield drop phenomenon depends strongly on the temperature with respect to T_g, and relatively low temperature promotes a higher $\Delta\sigma$[18−21]. The T/T_g value of $Ce_{60}Al_{15}Cu_{10}Ni_{15}$ alloy is 0.73 (T is room temperature), leading to a pronounced yield drop. As for the $Ce_{65}Al_{10}Cu_{10}Ni_{10}Nb_5$ alloy, the T/T_g value is 0.83, in which case the decrease in free volume controlled by diffusion becomes the predominant factor, and the $\Delta\sigma$ value is small, resulting in the inconspicuous serrated flow during loading. The T/T_g values of Zr- and Pd-based are much lower, only about 0.3−0.5 at room temperature. In this case, the plastic deformations of BMGs are fully localized into shear bands, without exhibiting homogenous deformation and yield drop, giving rise to the smooth *P-h* curves at high loading rates.

Fig. 3 shows representative surface morphologies of the indents of $Ce_{60}Al_{15}Cu_{10}Ni_{15}$ alloy after nanoindentation at various loading rates. Pile-up of the material in the form of semi-circular shear bands is observed at low loading rates (0.075 mN/s, Fig. 3(a)) around the indent, but not observed at higher loading rate (1 mN/s, Fig. 3(b)) . This indicates that the serrated flows in *P-h* curves at high rates do not correspond to the formation of multiple shear bands. Therefore, the serrations in *P-h* curves at high rates in $Ce_{60}Al_{15}Cu_{10}Ni_{15}$ alloy are not caused by the propagation of shear bands, but caused by the inhomogeneous flow (non-Newtonian flow) of alloy, depending strongly on T/T_g. $Ce_{60}Al_{15}Cu_{10}Ni_{15}$ alloy has a much lower T/T_g than $Ce_{65}Al_{10}Cu_{10}Ni_{10}Nb_5$ alloy, and tends to flow inhomogeneously. This should be the reason for the difference in deformation behavior between $Ce_{60}Al_{15}Cu_{10}Ni_{15}$ and $Ce_{65}Al_{10}Cu_{10}Ni_{10}Nb_5$ alloy at high loading rates.

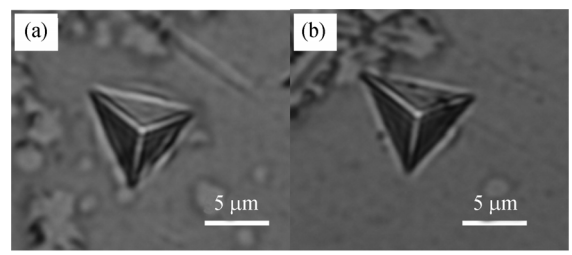

Fig. 3. The images of the morphology around the indents for $Ce_{60}Al_{15}Cu_{10}Ni_{15}$ alloy after nanoindentation at the loading rate of 0.075 mN/s (a) and 1 mN/s (b).

The strength (or hardness) of Zr-, Pd-based BMGs was independent of strain rate [22−24]. However, the hardness of the present $Ce_{60}Al_{15}Cu_{10}Ni_{15}$ and $Ce_{65}Al_{10}Cu_{10}Ni_{10}Nb_5$ alloys both increase with the loading rate (Fig. 2). This phenomenon is also related to the high

T/T_g of the two alloys. At a temperature near T_g, the deformation in BMGs contains viscoelastic and viscous flow modes, which are both time-dependent processes. Thereby, the maximum load needed to attain the designed indentation depth is higher at higher loading rates, as the viscoelastic and viscous flow are suppressed during the loading process. In other words, higher hardness will be observed at higher loading rates, while at the lower loading rate, viscoelastic deformation and viscous flow take place simultaneously during the slow loading process, resulting in a lower hardness. The tendency of hardness increasing with the loading rate during nanoindentation in the Ce-based BMGs at room temperature is consistent with deformation behavior of other BMGs at high temperature [19−21].

The creep displacement during the load holding segment of two Ce-based alloys is also caused by the viscoelastic deformation and the viscous flow. At higher loading rates, the plastic deformation occurs mainly during the load-holding segment at the maximum load, as the viscoelastic or elastic deformations are suppressed during the loading process, which leads to a pronounced creep displacement. But at the lower loading rate, the plastic deformation occurs mainly during the loading process, and its saturated value is almost reached before the beginning of the holding segment. As a result, the creep displacement increases with the increasing loading rate.

The strain rate sensitivity coefficient (m) is an important parameter with respect to plastic deformation, defined as

$$m = \frac{\Delta \log \sigma}{\Delta \log \dot{\varepsilon}},$$

where σ is stress, and $\dot{\varepsilon}$ is strain rate. Fig. 4 shows the double logarithm curves of the $\dot{\varepsilon}$ dependency of σ. In Fig. 4, the dashed lines are the linear fits of the experimental results, and the slope of those is m. The m value of $Ce_{60}Al_{15}Cu_{10}Ni_{15}$ and $Ce_{65}Al_{10}Cu_{10}Ni_{10}Nb_5$ alloy is 0.075 and 0.085 respectively, much lower than unit. Consequently, the plastic deformation in the two BMGs is still highly inhomogeneous and is localized in shear bands, though the plastic deformation of two Ce-based alloys contains viscoelastic and viscous flow. This is proved by the direct observation of the plastic deformation region under the indent [1)].

3 Conclusions

$Ce_{60}Al_{15}Cu_{10}Ni_{15}$ BMG shows smooth P-h curves at low loading rates and a distinct serrated flow at high loading rates during the loading process of nanoindentation, whereas $Ce_{65}Al_{10}Cu_{10}Ni_{10}Nb_5$ BMG exhibits a continuous plastic deformation at all the studied loading rates. The serrated flow during nanoindentation of the two Ce-based BMG is correlated to the yield drop phenomenon due to their high T/T_g values. $Ce_{60}Al_{15}Cu_{10}Ni_{15}$ and $Ce_{65}Al_{10}Cu_{10}Ni_{10}Nb_5$ BMGs both exhibit creep displacement and the tendency of the hardness increasing with loading rate, suggesting that the plastic deformation of the Ce-based BMGs involves viscoelastic and viscous flow. However, the plastic deformation during nanoindentation is still highly inhomogeneous and is localized in the shear bands, as is proved by their quite low strain rate sensitivity coefficients during nanoindentation.

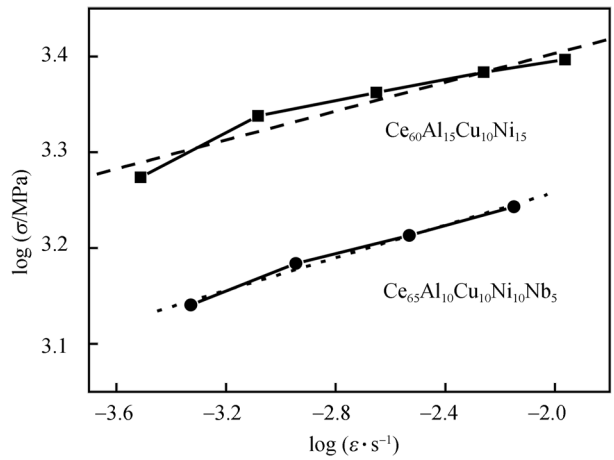

Fig. 4. Double logarithmic curves of strain rate ($\dot{\varepsilon}$) dependence of stress (σ) for $Ce_{60}Al_{15}Cu_{10}Ni_{15}$ and $Ce_{65}Al_{10}Cu_{10}Ni_{10}Nb_5$ BMGs.

Acknowledgements This work was supported by the National Natural Science Foundation of China (Grant Nos. 50571109, 10572142 & 10372103) and the Natural Science Fund for Outstanding Youth in Hunan Province (Grant No. 02JJYB010).

References

1 Inoue A. Stabilization of metallic supercooled liquid and bulk amorphous alloys. Acta Mater, 2000, 48: 279−306[DOI]

2 Guo F Q, Poon S J, Shiflet G J. Metallic glass ingots based on yttrium. Appl Phys Lett, 2003, 83: 2575−2577[DOI]

1) Zhang L C, Wei B C, Xing D M, et al. The characterization of plastic deformation in Ce-based bulk metallic glasses. Unpublished work

3 Wang W H, Dong C, Shek C H. Bulk metallic glasses. Mater Sci Eng R, 2004, 44: 45－89[DOI]

4 Schroers J, Johnson W L. Ductile bulk metallic glass. Phys Rev Lett, 2004, 93: 255506

5 Wright W J, Saha R, Nix W D. Deformation mechanisms of the Zr40Ti14Ni10Cu12Be24 bulk metallic glass. Mater Trans JIM, 2001, 42: 642－649[DOI]

6 Hufnagel T C, El-Deiry P, Vinci R P. Development of shear band structure during deformation of a Zr57Ti5Cu20Ni8Al10 bulk metallic glass. Scripta Mater, 2000, 43: 1071－1075[DOI]

7 Zhang Z F, He G, Eckert J, et al. Fracture mechanisms in bulk metallic glassy materials. Phys Rev Lett, 2003, 91: 045505[DOI]

8 Wang J G, Choi B W, Nieh T G, et al. Crystallization and nanoindentation behavior of a bulk Zr-Al-Ti-Cu-Ni amorphous alloy. J Mater Res, 2000, 15: 798－807

9 Nieh T G, Schuh C A, Wadsworth J, et al. Strain rate-dependent deformation in bulk metallic glasses. Intermetallics, 2002, 10: 1177－1182[DOI]

10 Wei B C, Zhang T H, Li W H, et al. Serrated plastic flow during nanoindentation in Nd-based bulk metallic glasses. Intermetallics, 2004,12:1239－1243

11 Golovin Y I, Ivolgin V I, Khonik V A, et al. Serrated plastic flow during nanoindentation of a bulk metallic glass. Scripta Mater, 2001, 45(8): 947－952[DOI]

12 Schuh C A, Nieh T G. A nanoindentation study of serrated flow in bulk metallic glasses. Acta Mater, 2003, 51: 87－99[DOI]

13 Schuh C A, Argon A S, Nieh T G, et al. The transition from localized to homogeneous plasticity during nanoindentation of an amorphous metal. Philos Mag A, 2003, 83: 2585－2597[DOI]

14 Argon A S. Plastic deformation in metallic glasses. Acta Metall, 1979, 27: 47－58[DOI]

15 Spaepen F. A microscopic mechanism for steady state inhomogenous flow in metallic glasses. Acta Metall, 1977, 25: 407－415[DOI]

16 Greer A L, Castellero A, Madge S V, et al. Nanoindentation studies of shear banding in fully amorphous and partially devitrified metallic alloys. Mater Sci Eng A, 2004, 375: 1182－1185[DOI]

17 Zhang B, Wang R J, Zhao D Q, et al. Properties of Ce-based bulk metallic glass-forming alloys. Phys Rev B, 2004, 70: 224208[DOI]

18 Schuh C A, Lund A C, Nieh T G. New regime of homogeneous flow in the deformation map of metallic glasses. Acta Metall, 2004, 52: 5879－5891

19 Kawamura Y, Shibata T, Inoue A. Stress overshoot in stress-strain curves of Zr65Al10Ni10Cu15 metallic glass. Appl Phys Lett, 1997, 71: 779－781[DOI]

20 Chen H S, Kato H, Inoue A. A fictive stress model and nonlinear viscoelastic behaviors in metallic glasses. Mater Trans JIM, 2001, 42: 597－605[DOI]

21 Nieh T G, Wadsworth J, Liu C T, et al. Plasticity and structural instability in a bulk metallic glass deformed in the supercooled liquid region. Acta Mater, 2001, 49: 2887－2896[DOI]

22 Mukai T, Nieh T G., Kawamura, Y et al. Dynamic response of a Pd40Ni40P20 bulk metallic glass in tension. Scripta Mater, 2002, 46: 43－47[DOI]

23 Subhash G, Dowding R J, Kecskes L J. Characterization of uniaxial compressive response of bulk amorphous Zr–Ti–Cu–Ni–Be alloy. Mater Sci Eng A, 2002, 334: 33－40[DOI]

24 Zhang Z F, Eckert J, Schultz L. Tensile and fatigue fracture mechanisms of a Zr-based bulk metallic glass. J Mater Res, 2003,18: 456－465